Accepted Manuscript

Sustainable synthesis of quaternary sulphides: The problem of the uptake of zinc in CZTS

Andrea Giaccherini, Adhara Baldassarre, Lorenzo Donini, Giovanni Orazio Lepore, Andrea Caneschi, Antonio De Luca, Massimo Innocenti, Giordano Montegrossi, Cucinotta Giuseppe, Werner Oberhauser, Luca Pardi, Maurizio Romanelli, Matteo Mannini, Francesco Di Benedetto

PII: S0925-8388(18)33875-1

DOI: 10.1016/j.jallcom.2018.10.201

Reference: JALCOM 48019

To appear in: *Journal of Alloys and Compounds*

Received Date: 14 May 2018

Revised Date: 4 September 2018

Accepted Date: 16 October 2018

Please cite this article as: A. Giaccherini, A. Baldassarre, L. Donini, G.O. Lepore, A. Caneschi, A. De Luca, M. Innocenti, G. Montegrossi, C. Giuseppe, W. Oberhauser, L. Pardi, M. Romanelli, M. Mannini, F. Di Benedetto, Sustainable synthesis of quaternary sulphides: The problem of the uptake of zinc in CZTS, *Journal of Alloys and Compounds* (2018), doi: https://doi.org/10.1016/j.jallcom.2018.10.201.

Sustainable synthesis of quaternary sulphides: the problem of the uptake of Zinc in CZTS

Giaccherini Andrea [1,2,3*], Baldassarre Adhara [2], Donini Lorenzo [1], Lepore Giovanni Orazio [4], Caneschi Andrea [3,5], De Luca Antonio [2,3], Innocenti Massimo [2,3], Montegrossi Giordano [3,6], Giuseppe Cucinotta [2,3], Oberhauser Werner [3,7], Pardi Luca [3,8], Romanelli Maurizio [1,3], Mannini Matteo [2,3], and Di Benedetto Francesco [1,3]

1 Department of Earth Sciences, University of Florence, Via La Pira 4, 50121, Firenze, Italy

2 Department of Chemistry, University of Florence, Via Lastruccia 3-13, 50019, Sesto Fiorentino (FI), Italy

3 INSTM Florence research unit, Via Lastruccia 3-13, 50019, Sesto Fiorentino (FI), Italy

4 IOM-CNR, c/o European Synchrotron Radiation Facility 71, avenue des Martyrs, 38043, Grenoble Cedex 9, France.

5 Department of Engineering, University of Florence, Via di S. Marta 3, 50139, Firenze, Italy

6 ICCOM-CNR, Via Madonna del Piano 10, 50019, Sesto Fiorentino (FI), Italy

7 IGG-CNR, Via La Pira 4, 50121, Firenze, Italy

8 IPCF-CNR, Via G. Moruzzi, 1 – 56124 Pisa, Italy

*andrea.giaccherini@unifi.it

kesterite, green chemistry, CZTS, thin films, photovoltaics.

Abstract

Quaternary semiconducting sulphides are promising and sustainable candidates to replace the silicon-based semiconduct-ing materials currently leading the market of the photovoltaic energy production. Recent efforts were paid to CZTS (Copper Zinc Tin Sulphides) semiconductors, due to their suitable electronic properties, the abundance in nature of their con-stituents, and the low toxicity. In this study, we synthetized $Cu_{3-x}Zn_xSnS_4$ samples by two different solvothermal approaches, with the aim of developing a sustainable synthetic route in the cradle-to-grave full life cycle assessment. These two routes are character-ized by either a single step, or a two-steps procedure and allow operating in mild conditions limiting the use of additional chemicals. A multi-technique characterization protocol has been adopted to evaluate chemical, structural and functional properties of the final products. The selected analyses demonstrated that, in both cases, members of the kesterite-kuramite solid solution series were obtained. Still, only in the case of the two steps approach pure Cu_2ZnSnS_4 samples can be synthe-

sized, whereas the single step synthesis yields Zn-poor samples. The optical characterization of the optimized CZTS material obtained with the two-steps approach revealed a band gap value (1.6 eV), in line with literature's values, confirming the suitability of this synthesis for the development of materials for photovoltaic applications.

1 Introduction

In recent times, materials science has been deeply involved in the field of renewable energy sources. Strong contributions have been given in the quest for the development of new devices for solar energy conversion. Main efforts concerned proposals and developments of new materials, able to increase the economic feasibility of the various solutions considered as alternatives to the traditional silicon-based technologies [1,2]. This research pursued the optimization of these newer generations of solar cell technologies by increasing the device performances and the improvement of the synthetic processes. The control on the reaction paths and their simplification, while tailoring the functional properties of these products, were constantly improved. Indeed, other aspects come out for their relevance, including the scaling of the approach, which enables an easy implementation from the laboratory to the production conditions, and the sustainability of the synthesis. Costs due to the use of rare/scarce raw materials, as well as the environmental consequences of the production and decommissioning are now important constraints [3,4]. In this context, the close control of energy costs associated to the synthesis is also a crucial task: a reduction of these costs will warrant an improvement in the net balance between energy return on the energy invested (EROEI) due the device realization [5].

CZTS (namely Cu_2ZnSnS_4) represents one of the most promising technologies, candidate for the development of sustainable solar cells due to their low toxicity and to the earth-abundance of the constituent elements [2]. Currently, the best performances in conversion efficiencies, obtained with a CZTS technology through three main processes at laboratory scale, span from the 12.6 % value obtained with hydrazine-assisted solution processes (reduced to 10.2 % without using this dangerous solvent) [6,7] to 10.6 %, achieved in vacuum process [8] and 8 %, obtained in electrochemical process [9]. Recently, some efforts were made to establish and improve the solvothermal approach, which is less energy costly compared to the co-evaporation and sputtering methods [10–16]. The effects of different parameters such as autoclave-based pressure control, solvents, temperatures, run duration and surfactants were explored [17–22]. However, simpler and less energy costly process could be explored (no surfactants, room pressure and more volatile solvent). Most of the literature seem to agree about the importance of the metal-thiourea complexes leading to the precipitation of CZTS in several different processes spanning from the solvothermal to thermalspray syntheses [23–29]. In the present study, several polycrystalline samples within the kesterite-kuramite solid solution ($Cu_{3-x}Zn_xSnS_4$) were obtained under a solvothermal approach. The structure of the two

endmembers are depicted in Figure 1 to show the structural similarities suggesting the occurrence of a solid solution as elsewhere discussed [30,31]. Two green and scalable solvothermal approaches based on the use of thiourea (TU) as a homogenous source of S^{2-} have been implemented to obtained such products. The two methods differ for the way the TU is added to the batch. The comparison between the two pure products, obtained so far, was performed by means of compositional, structural, magnetic and spectroscopic investigations.

2 Materials and methods

2.1 Synthesis. All syntheses of this study were performed using the following reactants: $CuCl_2 \cdot 2H_2O$ (Merck), $ZnCl_2$ (Alfa Aesar), $SnCl_2 \cdot 2H_2O$ (Riedel De Haën AG), thiourea (Merck), ethylene glycol (EG, 99%, Alfa Aesar), milliQ 18 MΩ water. The two different solvothermal methods share the use of TU as sulphide source. The first approach (**M1**) is adapted from the one-pot synthesis of kuramite, Cu_3SnS_4 [32], and pyrite, FeS_2 [33], nanopowders previously reported by some of us. In the present study we implemented the **M1** approach by putting proper amounts of metal chlorides and TU (see Supporting Information, Tab. S1) in a two-neck flask with ethylene glycol EG as a solvent under reflux at room pressure for 2 hours. The synthesis proceeds with the formation of a dark precipitate, which is collected at the end of the run, after having let the flask to cool at room temperature. Products are then centrifuged and washed for several times in ethanol to remove any impurity of unreacted moieties. The obtained powders are then air-dried. The second approach (M2) is a two-steps innovative method derived from the one successfully applied to the synthesis of metal doped ternary sulphides by Gusain et al. [34]. These authors exploited the decomposition of metal-TU complexes to achieve Ni^{2+}, Co^{2+}, Bi^{3+}, Sb^{3+} substituted Cu_3SnS_4 systems. In the present study, Me-TU complexes are obtained by adding opportune volumes of 0.4 M solutions of Me-chloride and TU, to realise the aqueous complexes having metal to ligand ratios equal to 1:3, 1:2 and 1:1 for Cu/TU, Zn/TU and Sn/TU, respectively [34–36]. Metal-TU complexes are obtained in the form of precipitates as chlorides by air-drying and/or rotary evaporation. The obtained Me-TU chlorides are then weighted in opportune proportions (see Supporting Information, Tab. S1) and used as reactants in the synthetic procedure. The run is carried out, as for **M1**, in a two-neck flask with EG as a solvent under reflux at room pressure for 2 hours, and the obtained precipitate is recovered after the reaction vessel is let cool to room temperature, centrifuged and washed in ethanol. Different run conditions were tested to optimize the synthesis strategy. The list of the performed runs is shown in Supporting Information (Tab. S1).

2.2 X-ray diffraction(XRD). The phase determination of the synthetic products was carried out through powder XRD, performed using a PANalytical X'PERT PRO powder diffractometer and employing Ni-filtered Cu Kα (1.54187 Å) radiation. The XRD patterns were registered at 1600 W (i.e. 40 kV, 40 mA) with a PIXcel detector on a rotating sample prepared on a

silicon wafer (zero-background sample holder) in the 2θ range 5–100°, applying a step size of 0.026° 2θ and a step counting time of 0.27 s. The XRD data were refined by means of a full-profile Rietveld algorithm, using the Fullprof software [37]. The same software was used to optimize the unit-cell parameter values, using a model in which the unit-cell parameters, the fractional coordinate of the sulphur in the CZTS structural model, the line width and a preferred orientation parameter, along [200], were kept free.

2.3 Scanning electron microscopy (SEM). Particle morphology was evaluated by means of SEM, at two different magnification levels (13500X and 33000X). The powder was mounted on standard aluminium sample holders with adhesive graphite tabs. To enhance the quality of the micrograph at high magnification, samples were carbon coated. Secondary-electron micrographs were obtained using a SEM ZEISS EVO MA15 as well as a Hitachi 2300 SEM microscope using in both cases 20 kV acceleration. The composition of the samples was determined by means of Energy Dispersive (EDS) Microanalysis using an Oxford INCA 250 and a NORAN NSS 300, Thermo Fisher Scientific, (Waltham, MA, USA) systems mounted respectively in the two above mentioned microscopes. The peaks were fitted by Gaussian curves applying the ZAF (atomic number absorption fluorescence) correction.

2.4 Electron Paramagnetic Resonance (EPR). Conventional EPR spectroscopy measurements were performed on powders inserted in amorphous silica tubes using a Teflon bag. Data were collected at room temperature using a Bruker ER 200D-SRC spectrometer operating at X-band (9.5 GHz) interfaced with DS/EPR software to a PC for data acquisition and handling. Operating conditions were 0.05 mT modulation amplitude and 100 kHz modulation frequency. Scan speed was set to 2.5 mT per second over a panoramic scan range 0–1 T and to 0.65 mT per second over a detail scan range 0.25-0.38 T. EPR investigations were carried out on the as-synthesized products without further manipulation.

2.5 Magnetometry. Magnetic investigations were carried out on the as-synthesized products. Magnetization measurements were performed in the 1.6–300 K temperature range using a Superconducting Quantum Interference Device (SQUID) magnetometer (MPMS Quantum Design) in the field-cooled (FC) mode at applied fields of 2.0 and 0.1 T. Corrections for diamagnetism, estimated from Pascal's constants [38], were applied.

2.6 Diffuse reflectance spectroscopy. The UV–vis-NIR diffuse reflectance spectrum of the as-synthesized products was measured using an Agilent Cary 300 spectrometer, equipped with a Labsphere PELA-1050 integration sphere. The DRS spectra were registered in the range 250–850 nm, at a step of 1 nm, counting 0.1 s per step. Reflectance of samples was compared with a standard fluoropolymer (Spectralon), characterized as the highest diffuse reflectance of any known material in this region of the spectrum.

2.7 X-ray Absorption Spectroscopy (XAS). XAS measurements at the K-edges of Cu and Zn were performed at the LISA beamline (BM-08) [39,40] of the European Synchrotron Radiation Facility (ESRF, Grenoble – France). The main optical features of this beamline were a fixed exit monochromator with a pair of Si [111] crystals, and a pair of Pd coated mirrors for harmonics rejection ($E_{cutoff} \approx 18$ keV). The measured samples included, besides the M2 sample from this study, a synthetic microcrystalline CZTS [41], as well as five natural samples: chalcocite, Cu_2S, covellite, CuS, djurleite, $Cu_{1.96}S$, digenite, Cu_9S_5 and anilite, Cu_7S_4. These natural samples were provided by the Mineralogical Section of the Natural History Museum of the University of Florence. Measurements were performed in the transmission mode. Samples were mixed with cellulose and pressed in pellets using an amount of material such as to keep the total absorption (μ) $\leq$1.5 above the edge. The energy sampling interval in the near edge region was 0.2 eV; spectra were acquired with a fixed k step of 0.025 $Å^{-1}$ up to a maximum k value of 13 and 15 $Å^{-1}$ for Cu and Zn, respectively. All samples were measured at 80 K. The software ATHENA [42] was used to calibrate energy and to average multiple spectra. Standard procedures [43] were followed to extract the structural EXAFS signal ($k\chi(k)$): pre-edge background removal, spline modelling of bare atomic background, edge step normalization, and energy calibration. Model atomic clusters centred on the absorber atom were obtained by ATOMS [44] using atomic coordinates taken from Bonazzi et al. [45]. EXAFS spectra were fitted through the ARTEMIS software [42] in the Fourier-Transform (FT) space.

3 Results

An XRD, morphological and semiquantitative compositional analysis were carried on all the samples obtained from both the method **M1** and **M2**. Conversely, a complete characterization of the best outocomes of methods **M1** and **M2** have been carried on samples M1_8 and M2_15 since they are the samples with the higher concentration of Zn obtained for each method. The analysis confirmed that method **M1** provides consistently monophasic $Cu_{3-x}Zn_xSnS_4$ materials, the Zn-content of which never exceeds 0.1 apfu (Tab. S2). Accordingly, the effect of adding Zn to the batch of reactants of the method **M1** results in the precipitation of kuramite and spurious associated phases. Conversely, the products provided by the method **M2** are regularly monophasic $Cu_{3-x}Zn_xSnS_4$, with a variable chemical composition being $0.5 \leq x \leq 1$ (Tab. S3).

3.1 Morphology, particle size, composition and structure. SEM-EDX analysis of samples from both **M1** and **M2** syntheses evidenced the presence of irregularly shaped aggregates of several microns (Fig. 2). They are constituted by smaller particles of spherical or tabular habitus having a size of the order of some hundreds of nanometres. Apparently, the latter are polydisperse with an anhedral morphology, suggesting that they could be polycrystalline and constituted by even smaller crystallites. The most striking feature is the absence of any appreciable difference in size and/or morphology between the products obtained by the two different synthetic routes, while a clear lack of Zn uptake occurring during the **M1** process (Tab. 1). This

feature appears even more relevant if one considers that almost all the existing literature on solvothermal CZTSs, obtained with different strategies, reports an analogous particle morphology [17–21,46,47] . The mean crystallite size has been evaluated on the basis of the effective width of the (112), (024) and (132) reflections (indexed according to the structural model of natural CZTS [48], Fig. 3) through the use of the Scherrer's equation [49]. The average crystallite sizes are 6.9 and 5.8 nm for the M1_8 and M2_15 samples, respectively. The change in size among the different reflections, < 15%, can be considered within the uncertainty of this determination. The crystallite growth appears isotropic in the different spatial directions. It is noteworthy that the crystallite size value is lower than the average size of the particles identified at the SEM investigations. This is in line with our previous reports [50] on the TEM-detected crystallite size of kuramite nanopowder obtained via a similar solvothermal approach. A Rietveld refinement of the experimental patterns of the two chosen samples has been successfully carried out in the framework of the CZTS structural model. The lattice parameters of the M2_15 and M1_8 samples are a = 5.444(3) Å and c = 10.88(1) Å and a = 5.445(1) Å and c = 10.618(5) Å, respectively. The values obtained for the lattice parameters compare very well with those of the natural CZTS (kesterite, a = 5.427 Å; c = 10.871 Å; JCPDS 26-0575 [48]), in the case of M2_15, and with those of the isostructural natural kuramite (a = 5.448 Å; c = 10.76 Å; JCPDS 33-0501 [51]), in the case of M1_8. This evidence is in excellent agreement with the fact that the M1_8 sample has a practically null nominal Zn-content, whereas the Zn-content in M2_15 sample is 1 apfu **(**Tab. S3**)**. A refinement carried out assuming a cubic sphalerite-like structural model (JCPDS 5-0566) yields even better results. Although not conclusively, these results are in support of a mixed occupancy of the cations in the available tetrahedral sites, suggested to play a relevant role in the semiconducting properties of the compound [17,52,53].

3.2 Probing the crystal chemistry: the Zn-S and Cu-S bonds. A further step into the study of the Zn uptake has been carried through the Cu K-edge XANES of the reference CZTS (kes750 in Figure 4) and of the M2_15 sample, together with some structurally related Cu sulphides standards of the Cu-S compositional field [54]. The spectra could contribute to confirm if the local structure around Zn atoms is compatible with CZTS excluding the precipitation of binary zinc sulphides during the **M2** synthesis (**Fig. 4**). Sample M2_15 shows great similarity with synthetic microcrystalline CZTS (kes750 – obtained by means of solid state synthesis [55]); besides, the "white-line" (roughly at 8984 eV) in the XANES regions of these two samples clearly distinguishes from the other Cu sulphides reported in Figure 4. EXAFS (at Cu and Zn K-edge) of Kes750 and M2_15 samples, along with the respective Fourier transforms are shown in Fig. 5a and b. The corresponding multiparameter fits are also reported in the same Figures 5 and the fit results in Table 2. It is worth to notice that the second shell signal is clearly present in Kes750 but it cannot be clearly observed in M2_15. This is in reasonable agreement with the lower ordering expected from the extremely small crystallites or with a non-homogeneous distribution of the Zn atoms (zoning) in the

CZTS structure of the M2_15 samples. Still, in sample M2_15, both Cu- and Zn-S bonds show distances extremely close to a CZTS structure (e.g. ref [52] and references therein) and result in the typical range of a four-fold coordination with S. EXAFS and XANES data thus strongly point towards the incorporation of both Cu and Zn in a CZTS structure in the M2_15 sample.

3.3 Magnetic properties: the undirect proof of the zinc uptake. All the data presented so far strongly support, but not conclusively prove, the Zn uptake by M2_15 sample in the CTZS structure. EPR and magnetometric measurements can probe the crystal chemistry of the Cu/Zn mixed occupancy sites in the M1_8 and M2_15 samples, excluding the Cu(II) presence in the M2_15 sample and ultimately confirming the Zn uptake in the **M2** method [9]. Indeed, the recorded EPR and magnetometric features for the M1_8 sample can be ascribed to the presence of about 1 apfu of Cu(II), necessary to achieve the charge balance in agreement to the stoichiometry reported in Table S3 (see Supporting Information). Conversely, the EPR spectrum of the M2_15 sample (Figure 6a) is characterized by the presence of two signals, one centred at ~314.7 mT, and relatively broad (peak-to-peak line width, ΔHpp, ~41.3 mT) and one very narrow (ΔHpp = 0.70(1) mT), centred at 339.42(1) mT. Under the adopted operating frequency, the latter field value is very close to that expected for a g = 2.0 signal. For this reason, we attribute this signal to an electron not belonging to a specific metal ion, but to a "free electron", i.e. to a colour or to a Frenkel centre. This feature, although unexpected, is not new for sulphides: Di Benedetto et al. [56] have already noticed a similar occurrence in synthetic tetrahedrite ($Cu_{12}SbS_{13}$), and its presence was related to the complex electronic structures of all sulphide minerals having nominally divalent Cu (as e.g. in covellite [57]). Concerning the broad signal, its spectral features undoubtedly point to the attribution to Cu(II). The average g-value, 2.16, as well as the asymmetry of the signal are closely resembling those already described in natural CZTS [41]. In the natural phase, the mass balance of the divalent cation in CZTS is usually achieved by solid solution among divalent cations stable under sulfidic conditions (i.e. Zn, Fe, Cd, Mn, …). Thus, the amount of Cu(II) in the natural sample can be considered largely subordinate to that of the other divalent cation.

The similarity of the present spectrum with that of the natural sample points to a similar context. Cu(II) is not an abundant species in M2_15 sample (Tab. 1) confirming that the mixed occupancy sites in the CZTS structure are almost completely occupied by Zn(II).

An esteem of the paramagnetic content of the sample, carried out under the assumption that the unique paramagnetic ion is Cu(II), was performed through SQUID magnetometric investigations. The sample is substantially diamagnetic in a large interval of temperatures between 298 and 100 K. For temperature lower than 100 K, the sample exhibits a weak paramag-

netism. This ambiguous behaviour can be explained considering that for a very weak paramagnet (i.e. a $Cu_{3-x}Zn_xSnS_4$ sample with $x < 0.5$) the correction for the diamagnetic χ for $T > 100$ K is of the same order of magnitude, or even greater, of the paramagneticy. A determination of the actual Cu(II) content is, under these circumstances, almost prevented. The low content of Cu(II) in the sample, while being in line with the evidences of the EPR spectroscopy, indirectly confirms the uptake of Zn(II) in the sulphide crystal 3.4 *Electronic proprieties: band gap.* DRS measurements were performed to estimate the band gap energy of M2_8 and M2_15 samples. The band gap value has been obtained by extrapolating, in the Tauc plot (Fig. 6b)[58], the linear part of the $(A \cdot E)^2$ function [59,60]. The value, 1.6 eV, obtained in both cases, compares well with the data reported in the literature [61] for microcrystalline CZTS (1.4–1.6 eV) and is in line with the ideal value of 1.5 eV[62–64]. The 100 meV discrepancy between the ideal and experimental value of the band gap is compatible with well-established limit of the Tauc's plot extrapolation for CZTS nanomaterials due to the effect of the tail states (or Urbach tails) [65,66]. The results here obtained are fully compatible with the optimal range for solar energy conversion (i.e., photovoltaic and photocatalytic applications).

4 Discussion

In this study we compare two different solvothermal methods (**M1** and **M2**) finding better results in the products of the **M2** syntheses. The main improvements reside in the different degree of zinc uptake in the sulphide structure and monophasicity of the products: the **M1** method provides $Cu_{3-x}Zn_xSnS_4$ samples containing up to 0.1 zinc apfu, whereas values up to 1 zinc apfu were achieved with the **M2** method.

Although the higher thermodynamic stability of CZTS over kuramite, the lack of a stoichiometric uptake of Zn in the **M1** synthesis even under the same thermodynamic conditions of **M2** syntheses suggests that a kinetic control may be operative during the reactive process in solution leading to the different outcomes of **M1** and **M2** processes.

Assuming that the precipitation of the multinary sulphides proceeds through the formation of multinary clusters[57] where Cu and Sn must be present, the ratio of Cu(II)/Zn(II) in the most favourable species (coordination compound or solvated ions) is probably the crucial variable to set the difference between the kuramite and CZTS. Indeed, the solubility of the binary sulphides sheds some light on the description of the reactive pathway from the solvated ionic species towards the precipitated multinary sulphide (i.e. kuramite or CZTS). ZnS (either cubic or hexagonal) is by far the most soluble among the binary sulphide considered as intermediates of reaction (i.e. SnS_2 and Cu_2S) [67–69]. This suggests, that during the **M1** synthesis, the sulphide anions produced by the decomposition of TU are immediately sequestered in the form of the corresponding Cu and Sn-bearing ternary clusters sulphides. Thus, the formation of Zn-bearing multinary clusters to form a quaternary phase or even the precipitation of ZnS is, to some extent, inhibited. Although, these considerations are ground on solubility data avail-

able only for water solutions; even taking into consideration that the solution water-EG is non-ideal [70], they qualitatively justify the different outcomes of the syntheses **M1** and **M2**.

Regarding the rate determining steps of the **M1** and **M2** process, the difference has to be related to the formation or the decomposition of the coordination compounds. To our knowledge it is not clear in the literature if the most favourable species for the formation of the multinary clusters are the thiourea coordination compounds or the solvated ions [17–29]. Hence, we can only infer that the formation or the decomposition of the metal coordination compounds with thiourea has to be considered the rate determining step for this reaction. A further relevant point concerns the chlorine content, highlighted in Table S3. This contamination, already observed in a previous report on solvothermal Fe-bearing kuramite[23], could be due either to the incorporation of chloride anions in the sulphide structure as side product of the solvothermal syntheses or to a co-precipitation of some metal chloride. Data in Table S3 point to the incorporation of Cl^- in the precipitate only in the case of the **M1** solvothermal synthesis. Conversely, no trace of chloride incorporation is found in the **M2** syntheses (Tab. S3), at least at the level of accuracy of the EDX analysis. This suggests that the **M2** synthesis occurs via a reaction path different from that of the **M1** process.

5 Conclusion

From the above mentioned considerations, the main difference between the one-pot **M1** and the two-steps **M2** approaches resides in the occurrence, during the former, of a solvation state for metals where the TU is not complexing them (at least not quantitatively). This difference largely influences the nature of the final products. The comparison with the known literature sheds light on the effect of the Zn counter ion in the uptake of Zn by the $Cu_{3-x}Zn_xSnS_4$ [17–29]. In particular, comparing with the scheme proposed by Bahramzadeh et al. [17] and concerning, among others, the precipitation from metal salts and TU in EG, we point out that in our case no evidence of the formation of organised structures (e.g. sheets, plates, rods) are observed, and only sub-spherical particles are detected. The production of solvothermal CZTS, with the nominal $Cu_{3-x}Zn_xSnS_4$ composition with $x \geq 0.5$, carried out through the **M2** method proved to be a procedure able to provide good nanopowder products, minimising both energy consumption (through short run duration and the lowest applicable temperature of synthesis) and environmental costs (through the removal of unnecessary chemicals during the synthesis). Moreover, both the two methods appear fully scalable to a reactor or even to a production level.

Author Contributions

All authors have given approval to the final version of the manuscript.

Funding Sources

This work has been partially funded through the MagHARPS project (Call RTD2016) funded by the University of Firenze. ESRF is gratefully acknowledged for provision of the synchrotron radiation and access to the facility.

Acknowledgment

The authors are grateful to Ferdinando Capolupo for his technical collaboration. XAS measurements were carried out during the 08-01 1033 experiment. M. Ulivi, D. Borrini and M. Paolieri are gratefully ackonwledged for their assistance during the SEM investigations at MEMA (Department of Earth Sciences - University of Florence). Stefano Martinuzzi and Stefano Caporali of the Department of Chemistry (University of Florence), are acknowledged for kindly granting the use of the SEM-EDX for the compositional analysis of the samples.

References

[1] S. Schorr, Structural aspects of adamantine like multinary chalcogenides, Thin Solid Films. 515 (2007) 5985–5991. doi:10.1016/j.tsf.2006.12.100.

[2] S.K. Wallace, D.B. Mitzi, A. Walsh, The Steady Rise of Kesterite Solar Cells, ACS Energy Lett. 2 (2017) 776–779. doi:10.1021/acsenergylett.7b00131.

[3] S.C. Riha, B.A. Parkinson, A.L. Prieto, Solution-Based Synthesis and Characterization of Cu 2 ZnSnS 4 Nanocrystals, J. Am. Chem. Soc. 131 (2009) 12054–12055. doi:10.1021/ja9044168.

[4] M.J. Thompson, K.J. Blakeney, S.D. Cady, M.D. Reichert, J. Del Pilar-Albaladejo, S.T. White, J. Vela, Cu2ZnSnS4Nanorods Doped with Tetrahedral, High Spin Transition Metal Ions: Mn2+, Co2+, and Ni2+, Chem. Mater. 28 (2016) 1668–1677. doi:10.1021/acs.chemmater.5b04411.

[5] A. Giaccherini, S. Cinotti, A. Guerri, F. Carlà, G. Montegrossi, F. Vizza, A. Lavacchi, R. Felici, F. Di Benedetto, M. Innocenti, Operando SXRD study of the structure and growth process of Cu2S ultra-thin films, Sci. Rep. In-press (2017).

[6] X. Liu, Y. Feng, H. Cui, F. Liu, X. Hao, G. Conibeer, D.B. Mitzi, M. Green, The current status and future prospects of kesterite solar cells: a brief review, Prog. Photovolt Res. Appl. 24 (2016) 879–898. doi:10.1002/pip.

[7] H. Azimi, Y. Hou, C.J. Brabec, Towards low-cost, environmentally friendly printed chalcopyrite and kesterite solar cells, Energy Environ. Sci. 7 (2014) 1829–1849. doi:10.1039/C3EE43865A.

[8] S. Giraldo, T. Thersleff, G. Larramona, M. Neuschitzer, P. Pistor, K. Leifer, A. Pérez-Rodríguez, C. Moisan, G. Dennler, E. Saucedo, Cu2ZnSnSe4 solar cells with 10.6% efficiency through innovative absorber engineering with Ge superficial nanolayer, Prog. PHOTOVOLTAICS Res. Appl. (2016). doi:10.1002/pip.

[9] D. Colombara, A. Crossay, L. Vauche, S. Jaime, M. Arasimowicz, P.P. Grand, P.J. Dale, Electrodeposition of kesterite thin films for photovoltaic applications: Quo vadis?, Phys. Status Solidi Appl. Mater. Sci. 212 (2015) 88–102. doi:10.1002/pssa.201431364.

[10] K. Ito, T. Nakazawa, Electrical and Optical Properties of Stannite-Type Quaternary Semiconductor Thin Films, Jpn. J. Appl. Phys. 27 (1988) 2094–2097. doi:10.1143/JJAP.27.2094.

[11] R. Lechner, S. Jost, J. Palm, M. Gowtham, F. Sorin, B. Louis, H. Yoo, R.A. Wibowo, R. Hock, Cu2ZnSn(S,Se)4 solar cells processed by rapid thermal processing of stacked elemental layer precursors, Thin Solid Films. 535 (2013) 5–9.

doi:10.1016/J.TSF.2012.10.042.

[12] H. Yoo, J. Kim, Growth of Cu2ZnSnS4 thin films using sulfurization of stacked metallic films, Thin Solid Films. 518 (2010) 6567–6572. doi:10.1016/J.TSF.2010.03.058.

[13] J. Márquez, M. Neuschitzer, M. Dimitrievska, R. Gunder, S. Haass, M. Werner, Y.E. Romanyuk, S. Schorr, N.M. Pearsall, I. Forbes, Systematic compositional changes and their influence on lattice and optoelectronic properties of Cu2ZnSnSe4 kesterite solar cells, Sol. Energy Mater. Sol. Cells. 144 (2016) 579–585. doi:10.1016/J.SOLMAT.2015.10.004.

[14] T. Tanaka, D. Kawasaki, M. Nishio, Q. Guo, H. Ogawa, Fabrication of Cu2ZnSnS4 thin films by co-evaporation, Phys. Status Solidi. 3 (2006) 2844–2847. doi:10.1002/pssc.200669631.

[15] K. Wang, O. Gunawan, T. Todorov, B. Shin, S.J. Chey, N.A. Bojarczuk, D. Mitzi, S. Guha, Thermally evaporated Cu2ZnSnS4 solar cells, Appl. Phys. Lett. 97 (2010) 143508. doi:10.1063/1.3499284.

[16] W.-C. Hsu, I. Repins, C. Beall, G. Teeter, C. DeHart, B. To, Y. Yang, R. Noufi, Growth kinetics during kesterite coevaporation, in: 2012 38th IEEE Photovolt. Spec. Conf., IEEE, 2012: pp. 000674–000677. doi:10.1109/PVSC.2012.6317699.

[17] S. Bahramzadeh, H. Abdizadeh, M.R. Golobostanfar, Controlling the morphology and properties of solvothermal synthesized Cu2ZnSnS4 nanoparticles by solvent type, J. Alloys Compd. 642 (2015) 124–130.

[18] M. Cao, Y. Shena, A mild solvothermal route to kesterite quaternary Cu2ZnSnS4 nanoparticles, J. Cryst. Growth. 318 (2011) 1117–1120.

[19] Y.L. Zhou, W.H. Zhou, Y.F. Du, M. Li, S.X. Wu, Sphere-like kesterite Cu2ZnSnS4nanoparticles synthesized by a facile solvothermal method, Mater. Lett. 65 (2011) 1535–1537. doi:10.1016/j.matlet.2011.03.013.

[20] M.-H. Jao, H.-C. Liao, M.-C. Wu, W.-F. Su, Synthesis and Characterization of Wurtzite Cu2ZnSnS4 Nanocrystals, Jpn. J. Appl. Phys. 51 (2012) 10NC30-1/3. doi:10.1021/ja9044168.

[21] M. Pal, N.R. Mathews, R.S. Gonzalez, X. Mathew, Synthesis of Cu2ZnSnS4 nanocrystals by solvothermal method, Thin Solid Films. 535 (2013) 78–82. doi:10.1016/j.tsf.2012.11.043.

[22] J.T. Han, Y.H. Huang, W. Huang, Solvothermal synthesis and magnetic properties of pyrite Co1-xFexS2 with various morphologies, Mater. Lett. 60 (2006) 1805–1808. doi:10.1016/j.matlet.2005.12.027.

[23] P. Prabeesh, K.V. Vysakh, I.P. Selvam, S.N. Potty, Cu_2ZnSnS_4 Thin Films by Dip Coating from Metal-Thiourea Precursor Solution: Effect of Sulphurization Temperature on the Formation and Structural, Optical and Electrical Properties, J. Electron. Mater. (2018) 1–7. doi:10.1007/s11664-018-6438-8.

[24] C. Jiang, Y.T. Hsieh, H. Zhao, H. Zhou, Y. Yang, Controlling Solid-Gas Reactions at Nanoscale for Enhanced Thin Film Morphologies and Device Performances in Solution-Processed $Cu_2ZnSn(S,Se)_4$ Solar Cells, J. Am. Chem. Soc. 137 (2015) 11069–11075. doi:10.1021/jacs.5b05819.

[25] J. Xu, Z. Hu, J. Zhang, W. Xiong, L. Sun, L. Wan, R. Zhou, Y. Jiang, C.-S. Lee, Cu_2ZnSnS_4 and $Cu_2ZnSn(S_{1-x}Se_x)_4$ nanocrystals: room-temperature synthesis and efficient photoelectrochemical water splitting, J. Mater. Chem. A. 5 (2017) 25230–25236. doi:10.1039/C7TA06628G.

[26] S.C. Riha, B.A. Parkinson, A.L. Prieto, Compositionally tunable $Cu_2ZnSn(S_{1-x}Se_x)_4$ nanocrystals: Probing the effect of Se-inclusion in mixed chalcogenide thin films, J. Am. Chem. Soc. 133 (2011) 15272–15275. doi:10.1021/ja2058692.

[27] S.N. Park, S.J. Sung, D.H. Son, D.H. Kim, M. Gansukh, H. Cheong, J.K. Kang, Solution-processed Cu_2ZnSnS_4 absorbers prepared by appropriate inclusion and removal of thiourea for thin film solar cells, RSC Adv. 4 (2014) 9118–9125. doi:10.1039/c3ra45441j.

[28] T. Chandel, V. Thakur, S. Halaszova, M. Prochazka, D. Haško, D. Velic, R. Poolla, Growth and Properties of Sprayed CZTS Thin Films, J. Electron. Mater. 47 (2018) 5477–5487. doi:10.1007/s11664-018-6433-0.

[29] T.K. Chaudhuri, D. Tiwari, Earth-abundant non-toxic Cu_2ZnSnS_4 thin films by direct liquid coating from metal-thiourea precursor solution, Sol. Energy Mater. Sol. Cells. 101 (2012) 46–50. doi:10.1016/j.solmat.2012.02.012.

[30] Y. Goto, F. Naito, R. Sato, K. Yoshiyasu, T. Itoh, Y. Kamihara, M. Matoba, Enhanced Thermoelectric Figure of Merit in Stannite − Kuramite Solid Solutions Cu 2+, Inorg. Chem. 52 (2013) 9861–9866.

[31] S. Rusakov, I. Chistyakova, A. Burkovsky, M. Gapochka, L. Evstigneeva, S. Schorr, Mössbauer study of isomorphous substitutions in Cu2Fe1-xCuxSnS4and Cu2Fe1-xZnxSnS4series, J. Phys. Conf. Ser. 217 (2010) 4–7. doi:10.1088/1742-6596/217/1/012038.

[32] F. Di Benedetto, D. Borrini, A. Caneschi, G. Fornaciai, M. Innocenti, A. Lavacchi, C.A. Massa, G. Montegrossi, W. Oberhauser, L.A. Pardi, M. Romanelli, Magnetic properties and cation ordering of nanopowders of the synthetic analogue of kuramite, Cu3SnS4, Phys. Chem. Miner. 38 (2011) 483–490. doi:10.1007/s00269-011-0421-8.

[33] A. Giaccherini, I. Colantoni, F. D'acapito, A. De Luca, F. Capolupo, G. Montegrossi, M. Romanelli, M. Innocenti, F. Di Benedetto, Green synthesis of pyrite nanoparticles for energy conversion and storage: A spectroscopic investigation, Eur. J. Mineral. 28 (2016) 611–618. doi:10.1127/ejm/2016/0028-2534.

[34] M. Gusain, P. Rawat, R. Nagarajan, Facile synthesis and optical properties of pure and Ni 2+ , Co 2+ , Bi 3+ , Sb 3+ substituted Cu 3 SnS 4, RSC Adv. 5 (2015) 43202–43208. doi:10.1039/C4RA17125J.

[35] A. Rosenhem, V.J. Meyer, Uber die Thiokarbamidverbindungen rweiwertiger Metallsalze, Zaac. 34 (1905) 13–27. doi:10.1002/zaac.19060490103.

[36] C.J. Doona, D.M. Stanbury, Equilibrium and Redox Kinetics of Copper(II)-Thiourea Complexes., Inorg. Chem. 35 (1996) 3210–3216. doi:10.1021/ic9502077.

[37] J. Rodriguez-Carvajal, Recent advances in magnetic structure determination by neutron powder diffraction + FullProf, Phys. B Condens. Matter. 192 (1993) 55–69.

[38] R.L. Carlin, Magnetochemistry, Springer-Verlag Berlin Heidelberg, 1986.

[39] A. Balerna, A. Grilli, S. Mobilio, A. Raco, V. Sciarra, V. Tullio, Gilda - general purpose italian beamline for diffraction and absorption - at esrf., Not Neutroni Luce Sincrotrone. 19 (2014) 14–23.

[40] F. D'Acapito, A. Trapananti, A. Puri, LISA: The Italian CRG beamline for x-ray Absorption Spectroscopy at ESRF, J. Phys. Conf. Ser. 712 (2016) 2–6. doi:10.1088/1742-6596/712/1/012021.

[41] G.P. Bernardini, D. Borrini, A. Caneschi, F. Di Benedetto, D. Gatteschi, S. Ristori, M. Romanelli, EPR and SQUID magnetometry study of Cu 2 FeSnS 4 (stannite) and Cu 2 ZnSnS 4 (kesterite), Phys. Chem. Miner. 27 (2000) 453–461. doi:10.1007/s002690000086.

[42] B. Ravel, M. Newville, ATHENA, ARTEMIS, HEPHAESTUS: Data analysis for X-ray absorption spectroscopy using IFEFFIT, J. Synchrotron Radiat. 12 (2005) 537–541. doi:10.1107/S0909049505012719.

[43] P.A. Lee, P.H. Citrin, P. Eisenberger, B.M. Kincaid, Extended x-ray absorption fine structure—its strengths and limitations as a structural tool, Rev. Mod. Phys. 53 (1981) 769.

[44] B. Ravel, ATOMS: Crystallography for the X-ray absorption spectroscopist, J. Synchrotron Radiat. 8 (2001) 314–316. doi:10.1107/S090904950001493X.

[45] P. Bonazzi, L. Bindi, P. Bernardini, S. Menchetti, A Model for the mechanism of incorporation of Cu, Fe and Zn in the Stannite – Kesterite series,Cu2FeSnS4 – Cu2ZnSnS4, 41 (2003) 639–647.

[46] K.-L. Huang, C.-H. Huang, W.-T. Lin, Y.-S. Fu, T.-F. Guo, Solvothermal synthesis and tunable bandgap of

Cu2(Zn1−xCox)SnS4 and Cu2(Fe1−xCox)SnS4 nanocrystals, J. Alloys Compd. 646 (2015) 1015–1022. doi:10.1016/J.JALLCOM.2015.05.176.

[47] C. Zn, F. Sns, T. Shibuya, Y. Goto, Y. Kamihara, M. Matoba, K. Yasuoka, From kesterite to stannite photovoltaics : Stability and band gaps of the Cu 2 (Zn , Fe) SnS 4 alloy, Appl. Phys. Lett. 104 (2014) 21912.

[48] S.R. Hall, J.T. Szymanski, J.M. Stewart, Kesterite, Cu2(Zn,Fe)SnS4, and stannite, Cu2(Fe,Zn)SnS4, structurally similar but distinct minerals, Can. Mineral. 16 (1978) 131–137. https://rruff-2.geo.arizona.edu/uploads/CM16_131.pdf (accessed February 20, 2018).

[49] a. L. Patterson, The scherrer formula for X-ray particle size determination, Phys. Rev. 56 (1939) 978–982. doi:10.1103/PhysRev.56.978.

[50] W.O. Reilly, V. Hoffmann, a C. Chouker, H.C. Soffel, a Menyeh, Magnetic properties of synthetic analogues of pyrrhotite ore in the grain size range 1 – 24 mm, Geophys. J. Int. (2000) 669–683.

[51] V.A. Kovalenker, Kuramite, Cu_3SnS_4, a new mineral of the stannite group, Int. Geol. Rev. 23 (1981) 365–370. doi:10.1080/00206818109455070.

[52] R. Bacewicz, J. Antonowicz, S. Podsiadło, S. Schorr, Local structure in Cu2ZnSnS4 studied by the XAFS method, Solid State Commun. 177 (2014) 54–56. doi:10.1016/J.SSC.2013.10.001.

[53] W. Zalewski, R. Bacewicz, J. Antonowicz, A. Pietnoczka, T.L. Evstigneeva, S. Schorr, XAFS study of kesterite, kuramite and stannite type alloys, J. Alloys Compd. 492 (2010) 35–38. doi:10.1016/j.jallcom.2009.11.158.

[54] R.J. Goble, Relationship Between Crystal Structure, Bonding and Cell Dimensions in the Copper Sulfides., Can. Mineral. 23 (1985) 61–76.

[55] G.P. Bernardini, P. Bonazzi, M. Corazza, F. Corsini, G. Mazzetti, L. Poggi, G. Tanelli, New data on the Cu2FeSnS4-Cu2ZnSnS4 pseudobinary system at 750C and 550C, Eur. J. Miner. 2 (1990) 219.

[56] F. Di Benedetto, G.P. Bernardini, C. Cipriani, C. Emiliani, D. Gatteschi, M. Romanelli, The distribution of Cu(II) and the magnetic properties of the synthetic analogue of tetrahedrite: Cu12Sb4S13, Phys. Chem. Miner. 32 (2005) 155–164. doi:10.1007/s00269-005-0449-8.

[57] R. a. D. Pattrick, J.F.W. Mosselmans, J.M.M. Charnock, K.E.R. England, G.R. Helz, C.D. Garner, D.J. Vaughan, The structure of amorphous copper sulfide precipitates: An X-ray absorption study, Geochim. Cosmochim. Acta. 61 (1997) 2023–2036. doi:10.1016/S0016-7037(97)00061-6.

[58] R.G. and A.V. J. Tauc, Optical Properties and Electronic Structure of Amorphous Germanium, Phys. Status Solidi B. 15 (1966) 627–637.

[59] S.I. Boldish, W.B. White, Optical band gaps of selected ternary sulfide minerals, Am. Mineral. 83 (1998) 865–871.

[60] M. Adelifard, H. Eshghi, M.M. Bagheri Mohagheghi, Synthesis and characterization of nanostructural CuS-ZnS binary compound thin films prepared by spray pyrolysis, Opt. Commun. 285 (2012) 4400–4404. doi:10.1016/j.optcom.2012.06.030.

[61] S. Botti, D. Kammerlander, M.A.L. Marques, Band structures of Cu2ZnSnS4 and Cu2ZnSnSe4 from many-body methods, Appl. Phys. Lett. 98 (2011) 241915. doi:10.1063/1.3600060.

[62] S. Siebentritt, S. Schorr, Kesterites-a challenging material for solar cells, Prog. Photovoltaics Res. Appl. 20 (2012) 512–519. doi:10.1002/pip.2156.

[63] D.B. Mitzi, O. Gunawan, T.K. Todorov, D.A.R. Barkhouse, Prospects and performance limitations for Cu-Zn-Sn-S-Se photovoltaic technology, Philos. Trans. R. Soc. A Math. Phys. Eng. Sci. 371 (2013) 20110432–20110432. doi:10.1098/rsta.2011.0432.

[64] N. Kamoun, H. Bouzouita, B. Rezig, Fabrication and characterization of Cu2ZnSnS4 thin films deposited by spray pyrolysis technique, Thin Solid Films. 515 (2007) 5949–5952. doi:10.1016/J.TSF.2006.12.144.

[65] S. Siebentritt, G. Rey, A. Finger, D. Regesch, J. Sendler, T.P. Weiss, T. Bertram, What is the bandgap of kesterite?, Sol. Energy Mater. Sol. Cells. 158 (2016) 126–129. doi:10.1016/j.solmat.2015.10.017.

[66] J.J.S. Scragg, J.K. Larsen, M. Kumar, C. Persson, J. Sendler, S. Siebentritt, C. Platzer Björkman, Cu-Zn disorder and band gap fluctuations in $Cu_2ZnSn(S,Se)_4$: Theoretical and experimental investigations, Phys. Status Solidi. 253 (2016) 247–254. doi:10.1002/pssb.201552530.

[67] J.W. Ball, D.K. Nordstrom, User's Manual for WATEQ4F, with revised thermodynamic data base and test cases for calculating speciation of major, trace, and redox elements in natural waters, U.S. Geol. Surv. Water-Resources Investig. Rep. 91–183 (1991) 1–188. http://wwwbrr.cr.usgs.gov/projects/GWC_chemtherm/pubs/wq4fdoc.pdf.

[68] J.W. Johnson, E.H. Oelkers, H.C. Helgeson, SUPCRT92: A software package for calculating the standard molal thermodynamic properties of minerals, gases, aqueous species, and reactions from 1 to 5000 bar and 0 to 1000??C, 1992. doi:10.1016/0098-3004(92)90029-Q.

[69] C.A.J. Appelo, D. Postma, Geochemistry, groundwater and pollution, Balkema, 2005.

[70] D.R. Cordray, L.R. Kaplan, P.M. Woyciesjes, T.F. Kozak, Solid - liquid phase diagram for ethylene glycol + water, Fluid Phase Equilib. 117 (1996) 146–152. doi:10.1016/0378-3812(95)02947-8.

Captions to figures and tables

Table 1. EDS semiquantitative microanalytical data of some of the investigated samples (expressed as wt%); formula coefficients are recalculated based on 8 atoms per formula unit. Nd-not detected. The row labelled "theo" presents the theoretical values.

Table 2. EXAFS multiparameter fit results for samples M2_15 and kes750 performed at the Cu (up) and Zn (down) K-edges (D.T. Debye Temperature).

Figure 1. A tilted perspective of the two endmembers of the $Cu_{3-x}Zn_xSnS_4$ solid solution (a) kesterite and (b) kuramite.

Figure 2. SEM micrographs of the M1_8 (a, c) and M2_15 (b, d) samples. Magnification: (a, b) 13500X; (c,d) 33000X.

Figure 3. Full XRD pattern of the M2_15 sample; reflections are indexed according to the kesterite crystal structure, JCPDS 26-0575 [48].

Figure 4. Comparison of normalized XANES spectra measured at Cu K-edge for samples M2_15 and Kes750 with those of various Cu sulphides. M2_15 is a spectrum of the sample obtained by means of the **M2** method, Kes750 is a synthetic CZTS obtained by means of a solid state synthesis [55] and the other spectra refer to natural samples provided by the Mineralogical Section of the Natural History Museum of the University of Florence.

Figure 5. Cu and Zn K-edge EXAFS (left) and Fourier transform (right) of M2_15 and Kes750 sample. Graphs in a) and b) refer to the Cu and Zn K edges, respectively. Experimental data are reported as black lines while red lines represent fits.

Figure 6. a) X-band EPR spectrum of the M2_15 sample, registered at room temperature, b) Tauc plot derived from the DRS spectrum of the M2_15 sample.

Synthesis	S (wt%)	Cu (wt%)	Zn (wt%)	Sn (wt%)	Cl (wt%)	S (apfu)	Cu (apfu)	Zn (apfu)	Sn (apfu)	Cl (apfu)
M1_8	31.5(4)	40.1(5)	1.9(3)	25.8(4)	0.8(1)	4.18	2.68	0.12	0.92	0.09
M2_15	27.1(3)	27.7(6)	15(1)	30.1(8)	Nd	3.83	1.98	1.05	1.15	-
theo	29.2	28.9	14.9	27.0	0.0	4	2	1	1	0

	Amp	Shell	R(Å)	σ^2(Å^{-2})	D.T. (K)	Amp	Shell	R(Å)	σ^2(Å^{-2})	D.T. (K)
Cu K-edge						Zn K-edge				
kes750	0.71(5)	4 S	2.311(5)	0.005(1)	-	0.79(8)	4 S	2.339(5)	0.003(1)	-
		8 (Cu,Zn)	3.883(8)	-	143(9)		8 (Cu,Zn)	3.847(8)	-	155(13)
		4 Sn	3.883(8)	-	//		4 Sn	3.847(8)	-	//
		4 S	4.50(1)	-	189(18)		4 S	4.46(1)	-	245(37)
		8 S	4.58(1)	-	//		8 S	4.54(1)	-	//
M2	0.75(5)	4 S	2.300(5)	0.006(1)	-	0.92	4 S	2.339(5)	0.007(1)	-

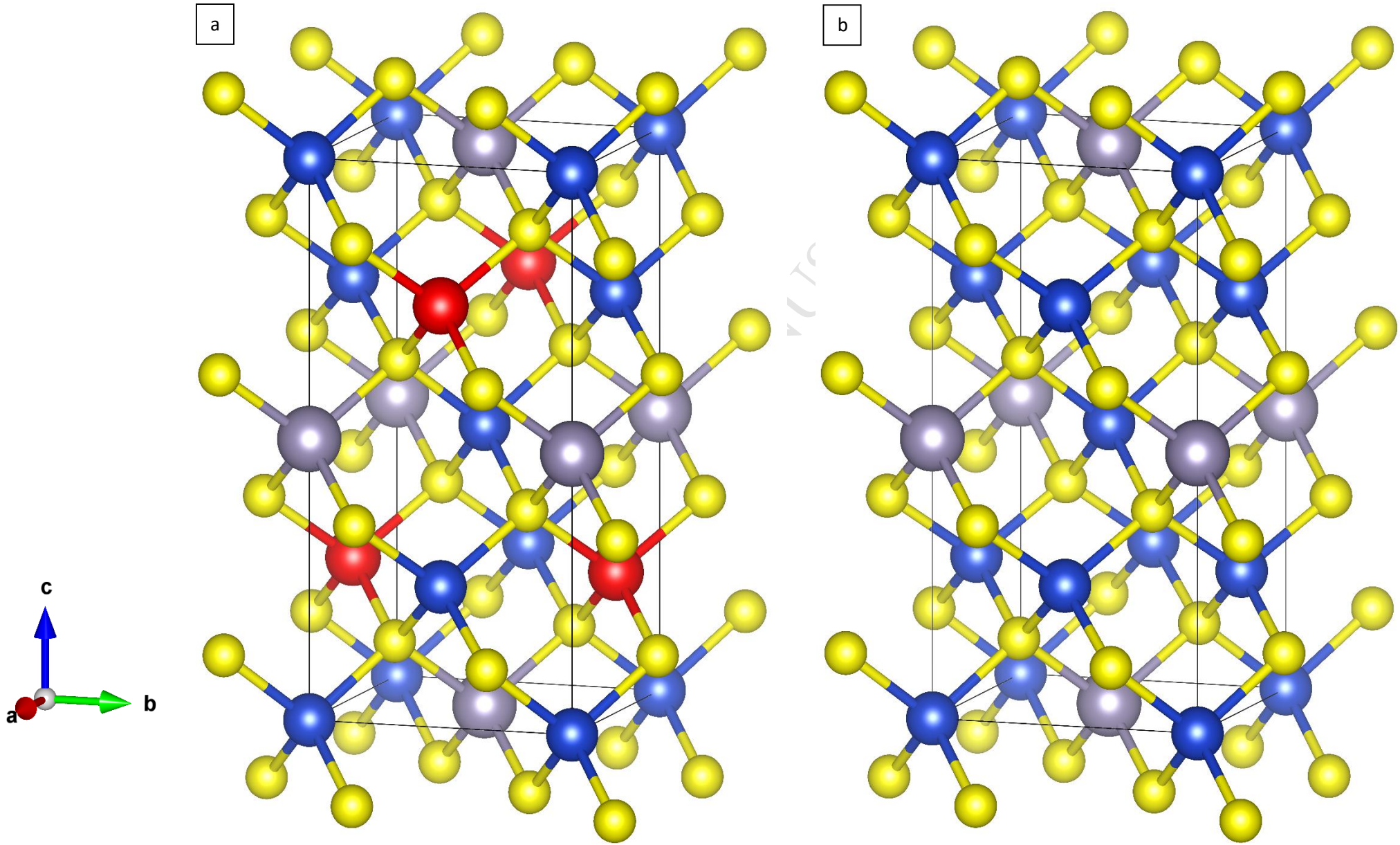
a
b
c
b
a

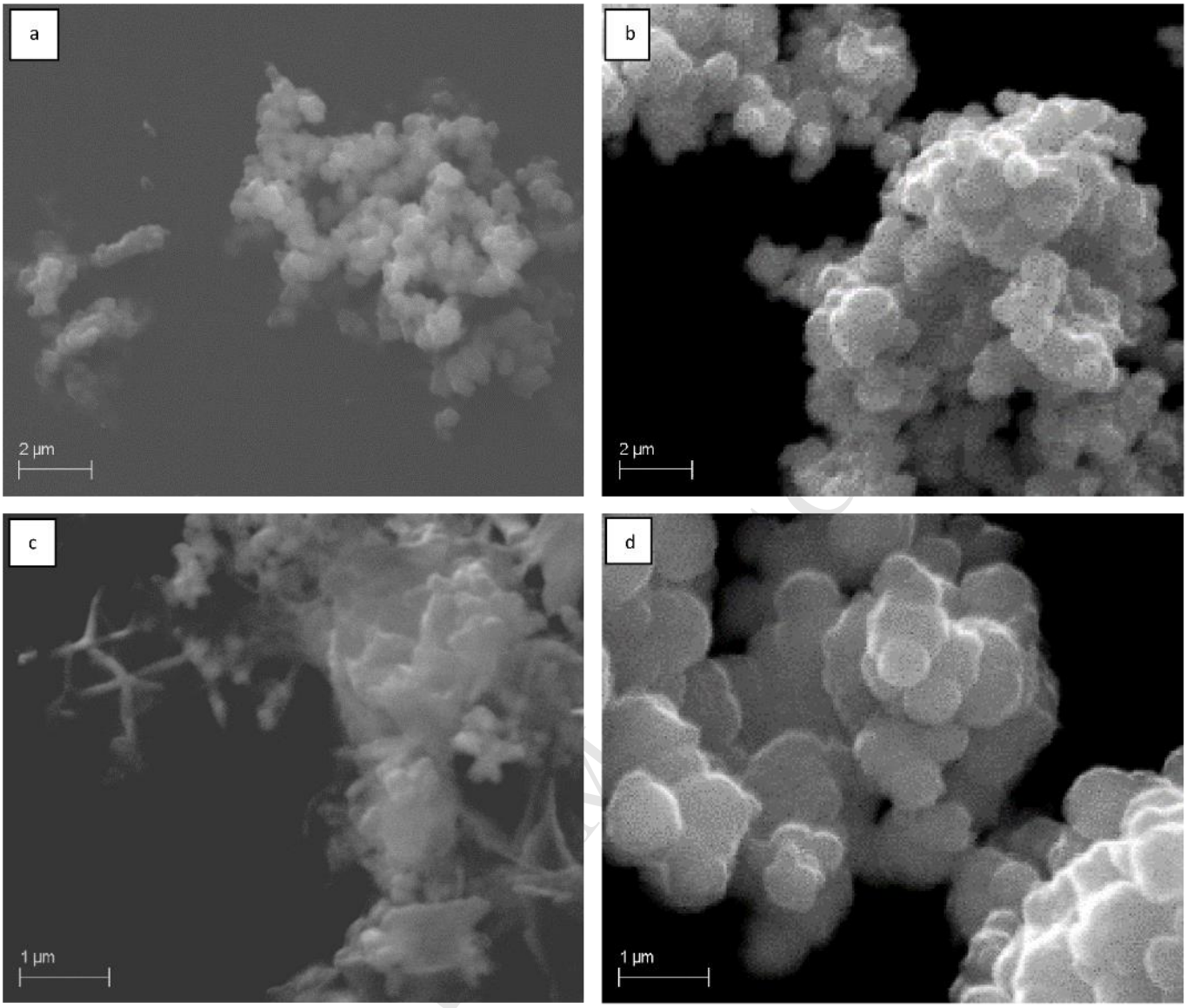

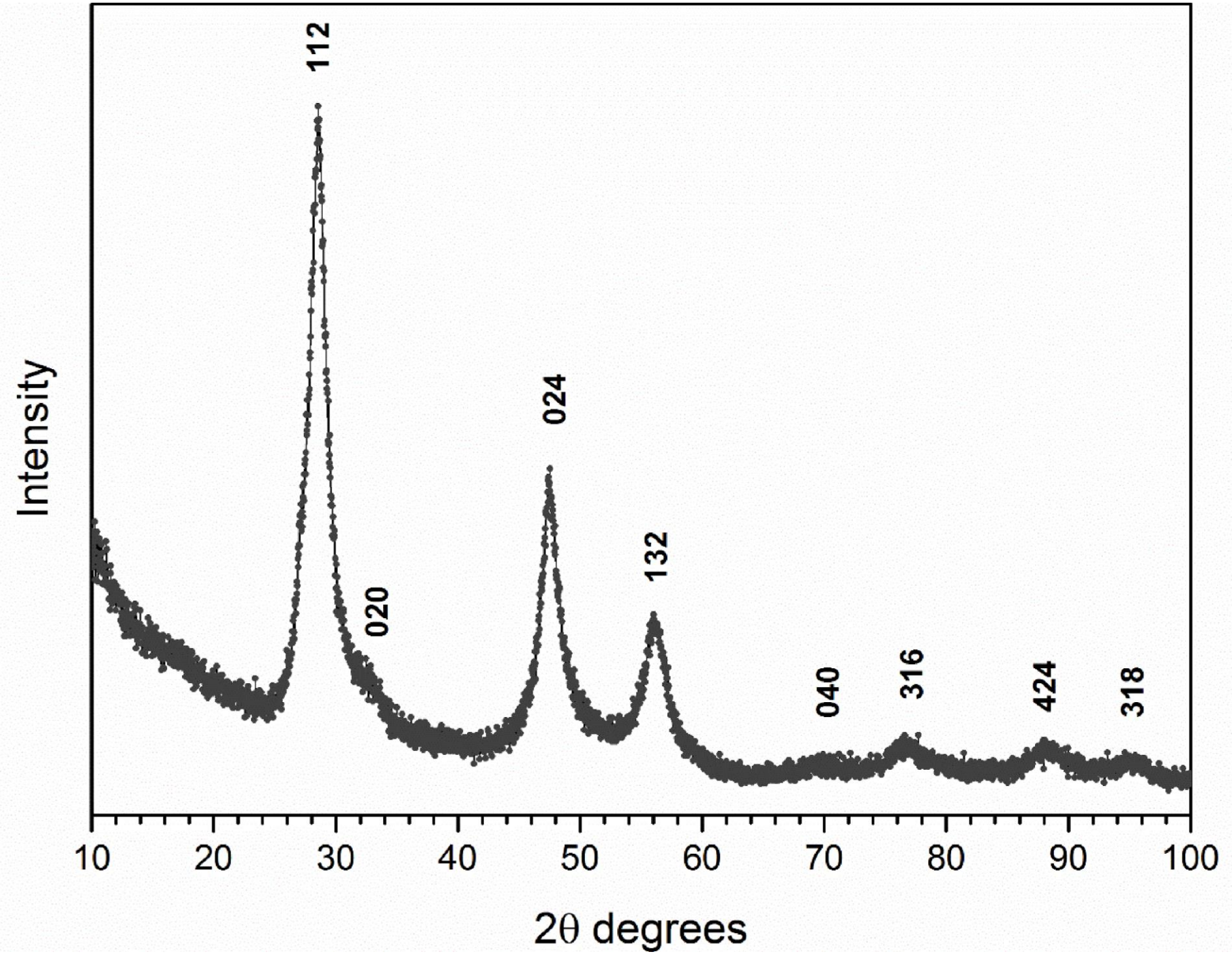
Intensity
112
020
024
132
040
316
424
318
10
20
30
40
50
60
70
80
90
100
2θ degrees

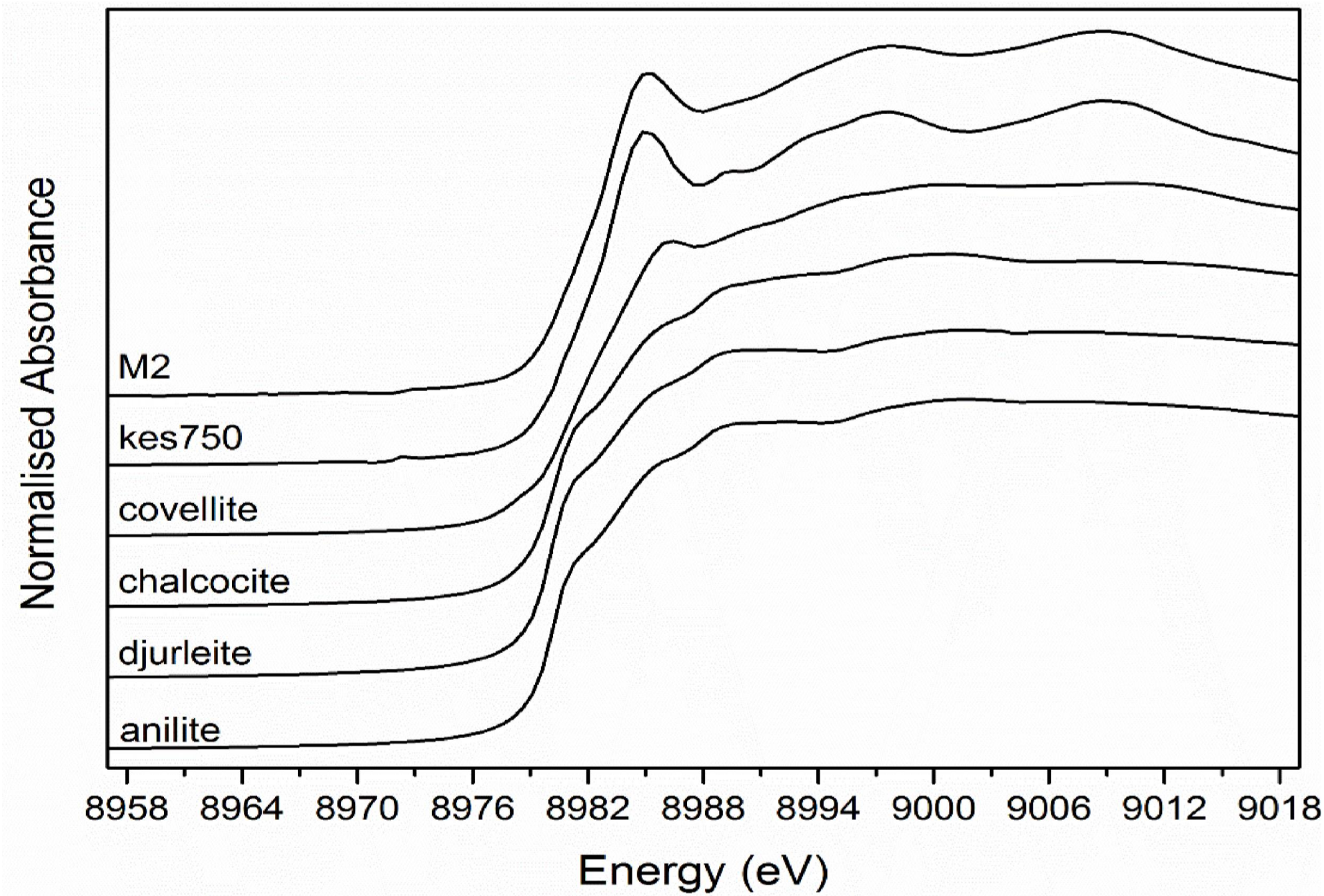

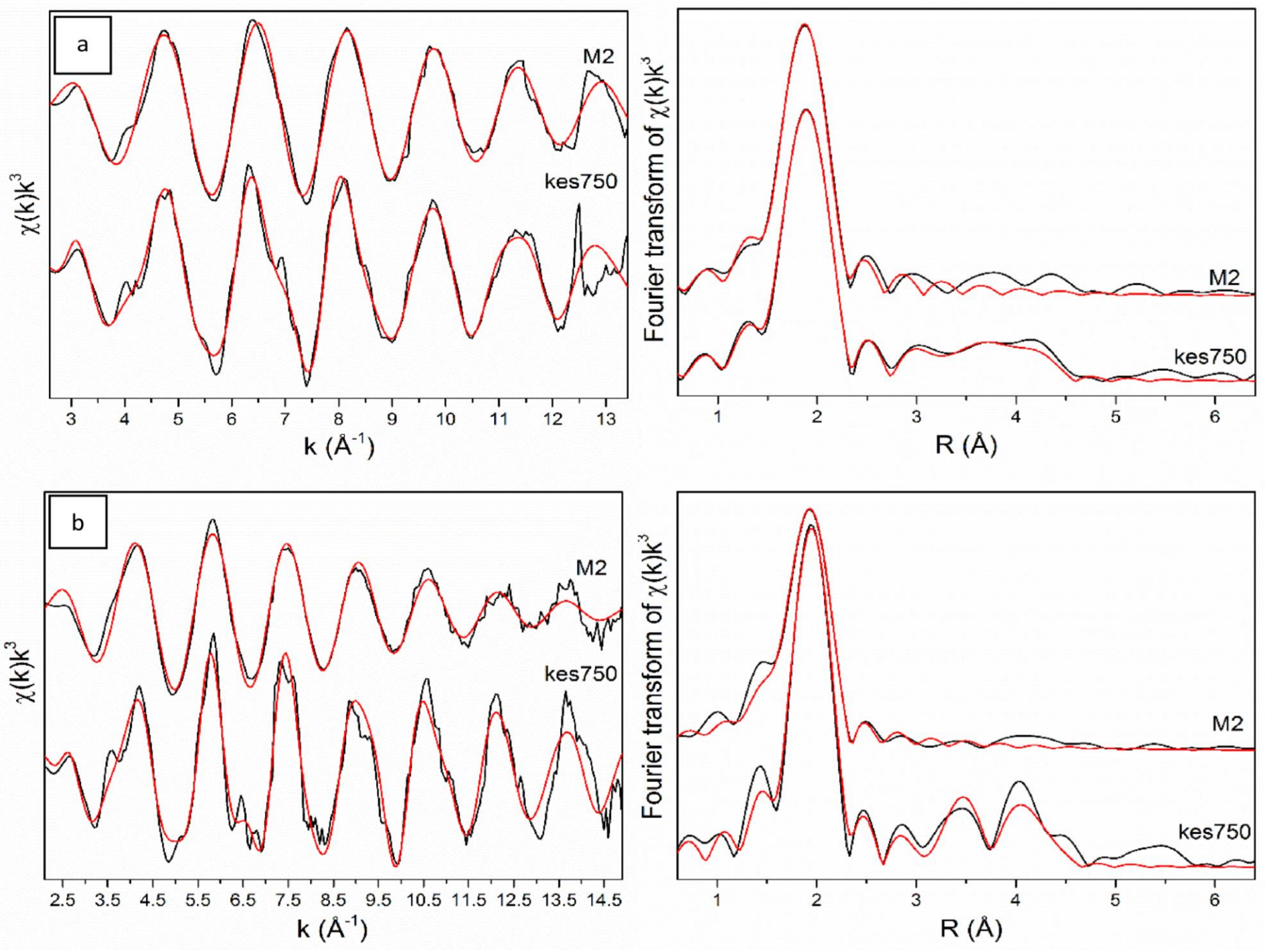
a
M2
kes750
χ(k)k³
k (Å⁻¹)
Fourier transform of χ(k)k³
R (Å)
b
M2
kes750
χ(k)k³
k (Å⁻¹)
Fourier transform of χ(k)k³
R (Å)

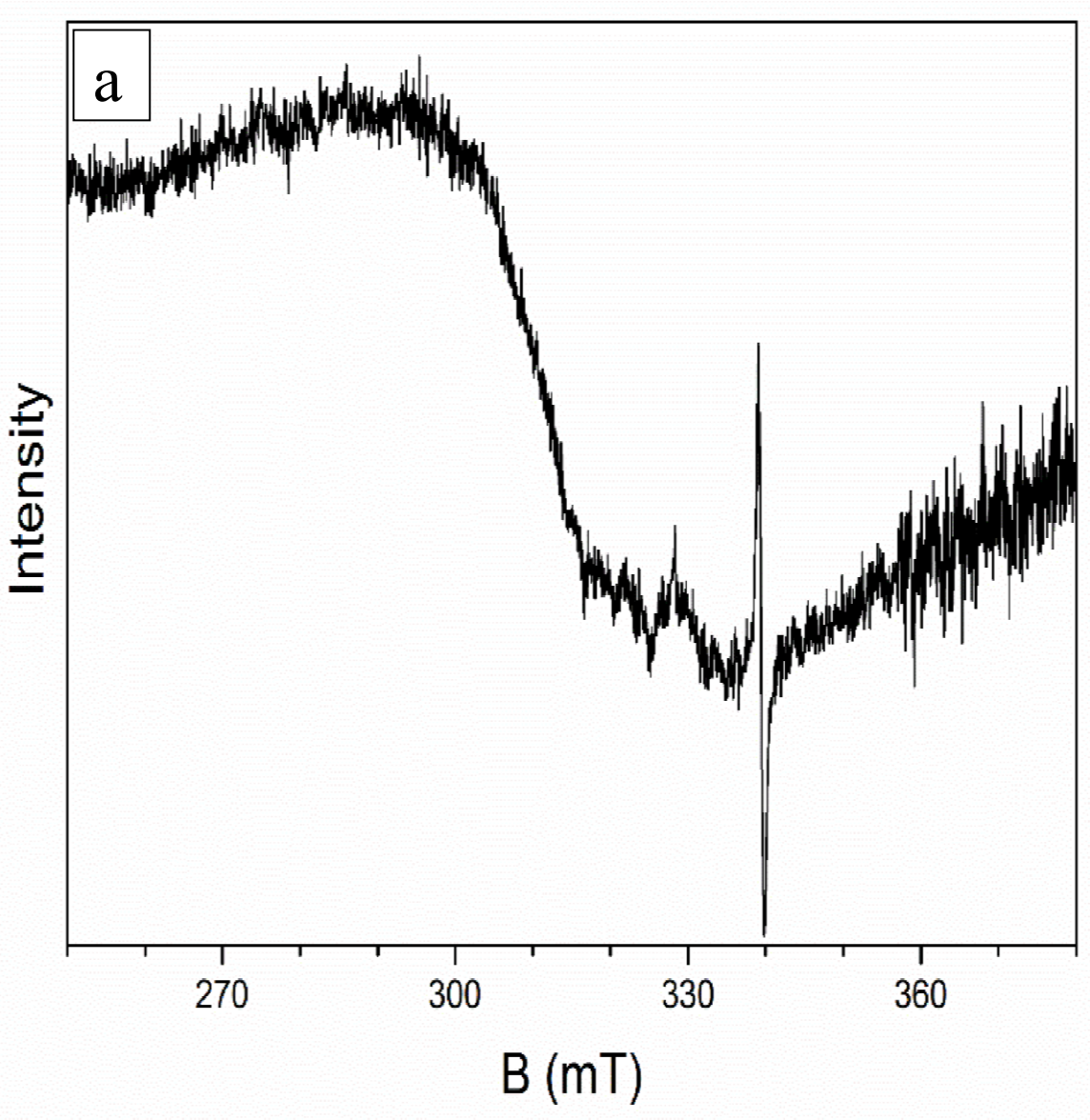
a
Intensity
270
300
330
360
B (mT)

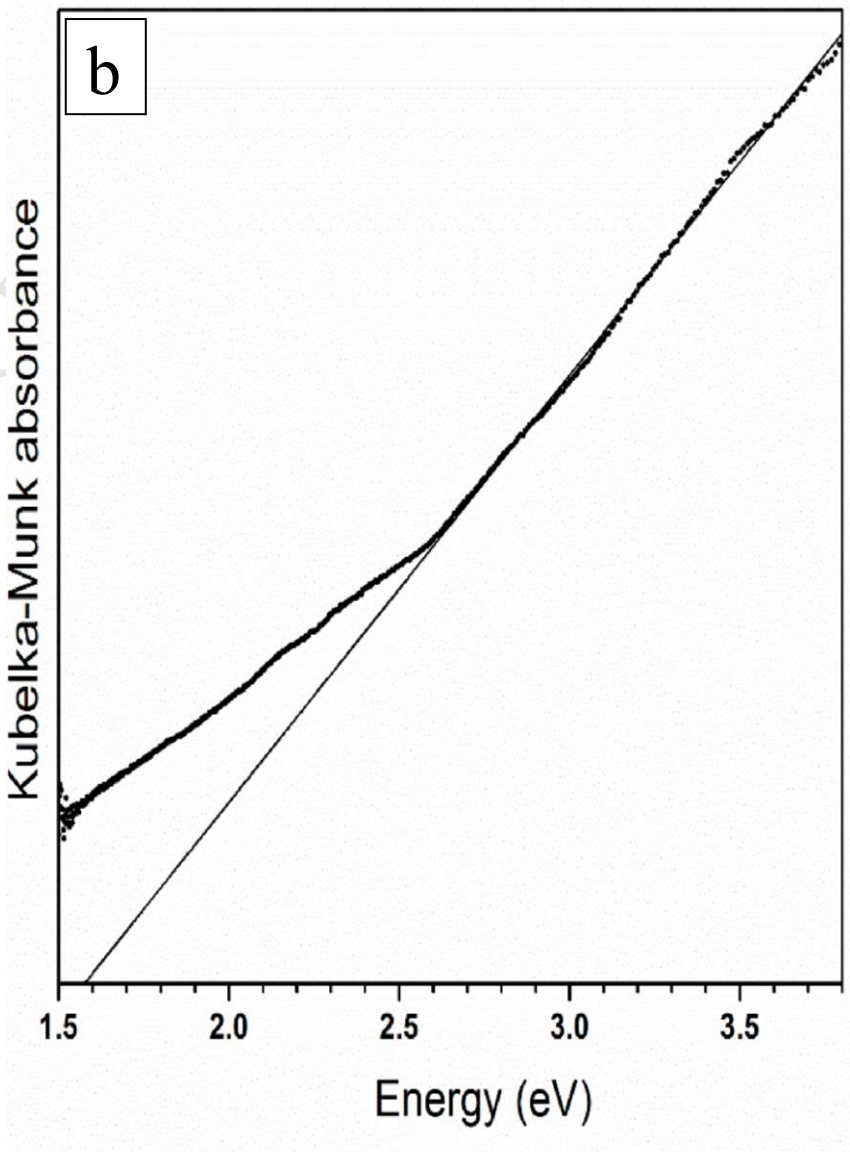
b
Kubelka-Munk absorbance
1.5
2.0
2.5
3.0
3.5
Energy (eV)

Highlights

- Synthesis of Cu_2ZnSnS_4 without surfactant and under mild conditions
- Cu_2ZnSnS_4 synthesis exploiting metal thiourea complexes as precursors
- Nature of the chemical limitations in uptaking Zn under this approach
- Crystal chemistry, composition and properties of the best product